This is the accepted manuscript made available via CHORUS. The article has been published as:

Observational constraint on axion dark matter with gravitational waves

Takuya Tsutsui and Atsushi Nishizawa

Phys. Rev. D **106**, L081301 — Published 10 October 2022

DOI: 10.1103/PhysRevD.106.L081301

Observational constraint on axion dark matter with gravitational waves

Takuya Tsutsui[1, 2] and Atsushi Nishizawa[1]

[1] *Research Center for the Early Universe (RESCEU), Graduate School of Science, The University of Tokyo, Tokyo 113-0033, Japan*

[2] *Department of Physics, Graduate School of Science, The University of Tokyo, Tokyo 113-0033, Japan*

(Dated: September 7, 2022)

Most matter in the Universe is invisible and unknown, which is called dark matter. A candidate of dark matter is axion, which is an ultra-light particle motivated as a solution for the CP problem. Axions form clouds in a galactic halo, amplify, and delay a part of gravitational waves propagating in the clouds. The Milky Way is surrounded by the dark matter halo composed of a number of axion patches. Thus, the characteristic secondary gravitational waves are always expected right after the reported gravitational-wave signals from compact binary mergers. In this paper, we derive a realistic amplitude of the secondary gravitational waves. Then we search the gravitational waves having the characteristic time delay and duration with a method optimized for them. We find no significant signal. Assuming the axions are dominant component of dark matter, we obtain the constraints on the axion coupling to the parity violating sector of gravity for the mass range, $[1.7\times10^{-13}, 8.5\times10^{-12}]$ eV, which is at most ~ 10 times stronger than that from Gravity Probe B.

I. INTRODUCTION

Most matter in the universe is invisible, which is called dark matter. Many candidates have been considered for dark matter. A candidate is quantum chromodynamics (QCD) axion [1] which is a pseudo Nambu-Goldstone boson introduced to resolve the CP problem. The CP problem is that many experiments, especially the measurements of the neutron electric dipole moment [2], prefer that the electric charge conjugate $\mathcal{C}$ and the parity $\mathcal{P}$ symmetries are conserved, which requires fine-tuning in the QCD theory. Furthermore, the existence of axions is also expected from the string theory [3], which is called string axion. The mass of the string axion ranges widely because it depends on the way of the compactification of the extra dimensions. Thus we should search for a broad mass range for both axions.

Although axions were historically introduced in the standard model of particle physics, axions have been searched often with electromagnetic (EM) interaction in the laboratory experiments [4, 5] and in astrophysics through the observations of supernovae [6] and active galactic nuclei [7]. Also the cosmological evolution of axions has been studied [8–16]. Many search methods and recent constraints are reviewed in [17–19].

Axions can also interact with gravity. Then, similar to the coupling to, for example, an electromagnetic field tensor in the QCD axion Lagrangian, we consider the Chern-Simons (CS) interaction term coupled to axions, that is, the axion nonminimal coupling to a Riemann tensor [20]. The additional term is the simplest coupling of a pseudo-scalar field to gravity, that is, the one appears in the CS gravity, which is a low-energy effective theory of parity violating extension of GR [20]. The CS coupling of axions have been searched in [21–33]. Especially, in the previous study [33], the measurement of the frame-dragging effect by Gravity Probe B around the Earth constrained the coupling, $\ell \lesssim 10^8$ km.

If axions interact with gravity through the CS term, gravitational waves (GWs) induce axion decay into gravitons [34]. If dark matter in the Milky Way (MW) is composed of axions, the propagating GWs are amplified and delayed. Since axions are expected to be cold dark matter in the MW halo, the GWs from the axion decay are almost monochromatic. Therefore, axions through the interaction generate characteristic secondary GWs whose features depend on the axion mass and the coupling to the parity violating sector of gravity [32].

In this paper, we search the monochromatic secondary GWs induced by primary GWs from coalescences of binary neutron stars (BNS) and binary black holes (BBH) in the observational data of GW detectors[1]. Our method is optimized for the time delay and the signal duration. Then, from no detection of the axion signal, we constrain the coupling constant, improving the upper limit from Gravity Probe B.

The organization of this article is as follows. In Sec. II, we review the properties of the secondary GWs generated by axion decay. We show the method we analyze GW data in Sec. III and the results in Sec. IV. We discuss the results and future prospects in Sec. V. Finally, Sec. VI is devoted to a summary.

In this paper, we use the natural unit $\hbar = c = 1$.

II. PROPERTIES OF SECONDARY GRAVITATIONAL WAVES

In this section, we briefly review the axion decay and enhancement of a GW in the MW halo, following Jung et

[1] Recently the possibility to search for axion dark matter through neutrino oscillation and a stochastic GW background was pointed out in [35].

al. [32], and enumerate the characteristic quantities for axions that we use later in the search. The Lagrangians are

$$S = S_{\rm EH} + S_a + S_{\rm CS}, \tag{1}$$

$$S_{\rm EH} = \frac{1}{16\pi G}\int d^4x\sqrt{-g}R, \tag{2}$$

$$S_a = -\int d^4x\sqrt{-g}\left(\frac{1}{2}\nabla_\mu a\nabla^\mu a + \frac{m_a^2}{2}a^2\right), \tag{3}$$

$$S_{\rm CS} = \frac{\ell^2}{16\sqrt{2\pi G}}\int d^4x\sqrt{-g}a^*RR, \tag{4}$$

where ℓ is the axion coupling constant in the parity violating sector of gravity, m_a is the axion mass, a is the axion field, and ${}^*RR$ is the Pontryagin density.

A. Characteristic quantities

A GW propagating through the MW halo composed of the axion dark matter with mass m_a produces secondary GWs which are almost monochromatic. The resonance frequency $f_{\rm res}$ is

$$f_{\rm res} = \frac{1}{2\pi}\frac{m_a}{2} = 12\,{\rm Hz}\left(\frac{m_a}{10^{-13}\,{\rm eV}}\right), \tag{5}$$

and its width is

$$\begin{aligned}\Delta f_{\rm res} =& 2f_{\rm res}\Delta v\\ =& 2.4\times10^{-2}\,{\rm Hz}\left(\frac{m_a}{10^{-13}\,{\rm eV}}\right)\left(\frac{\Delta v}{10^{-3}}\right),\end{aligned} \tag{6}$$

where Δv is a velocity dispersion of dark matter [36]. From Eq. (5), the LIGO [37, 38] sensitive band, 20 Hz – 1024 Hz, corresponds to $1.7\times10^{-13}\,{\rm eV} < m_a < 8.5\times10^{-12}\,{\rm eV}$. Therefore around a detected GW from compact binary coalescence (CBC), we can find the GW spectrum with a peak at only $f_{\rm res}$. The signal duration of the secondary GWs is roughly given by the inverse of the line width:

$$\begin{aligned}\Delta t_{\rm duration} =& \frac{1}{\Delta f_{\rm res}} = \frac{2\pi}{m_a\Delta v}\\ =& 41\,{\rm s}\left(\frac{10^{-13}\,{\rm eV}}{m_a}\right)\left(\frac{10^{-3}}{\Delta v}\right).\end{aligned} \tag{7}$$

The MW is composed of many coherent clouds of axion dark matter whose size is about the coherent length $L_{\rm c}$ defined by

$$\begin{aligned}L_{\rm c} :=& \frac{2\pi}{m_a\Delta v}\\ =& 4.0\times10^{-7}\,{\rm pc}\left(\frac{10^{-13}\,{\rm eV}}{m_a}\right)\left(\frac{10^{-3}}{\Delta v}\right).\end{aligned} \tag{8}$$

We note that the factor of 2π is different from the definition in [32]. Then, the following quantities including L_c are modified from those in [32] by the factor of 2π.

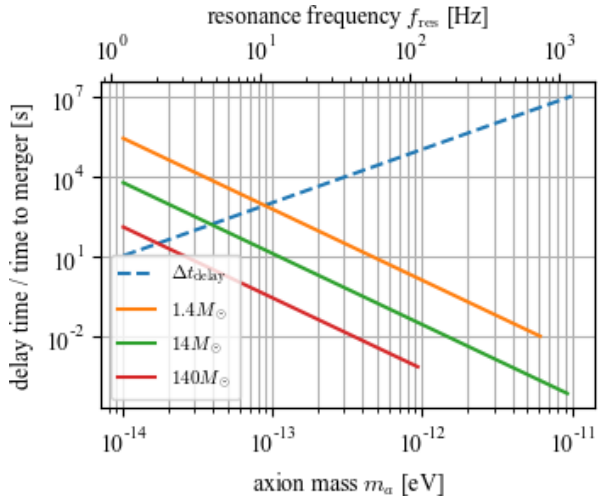


FIG. 1. The signal delay $\Delta t_{\rm delay}$ (dashed line) and the time to merger for various equal-mass binaries (solid lines) as a function of m_a for $\ell_{\rm eff} = 10^8$ km, $R = 100$ kpc, $\Delta v = 10^{-3}$, and $\rho_{\rm DM} = 0.3\,{\rm GeV/cm^3}$. Solid lines are plotted up to the innermost stable circular orbit (ISCO) frequency of a Schwarzchild BH for BNS of $1.4\,{\rm M}_\odot$–$1.4\,{\rm M}_\odot$ and their merger frequencies for other BBH.

The time-averaged group velocity of a GW in the axion clouds, $\bar{v}_g$, is

$$\bar{v}_g = 1 - \frac{1}{3}\left(\frac{\sqrt{\pi G\rho_a}\ell^2 m_a^2}{2}L_{\rm c}\right)^2. \tag{9}$$

Assuming that the MW halo is spherical symmetric and its radius is $R\sim100$ kpc, we can derive the delay time of the secondary GWs from the primary GW:

$$\begin{aligned}\Delta t_{\rm delay} =& \frac{R}{\bar{v}_g} - \frac{R}{c}\\ \simeq& \frac{\pi^3 R}{3}\frac{G\rho_a\ell^4 m_a^2}{\Delta v^2}\\ =& 1.1\times10^3\,{\rm s}\left(\frac{R}{100\,{\rm kpc}}\right)\left(\frac{10^{-3}}{\Delta v}\right)^2\left(\frac{\ell_{\rm eff}}{10^8\,{\rm km}}\right)^4\\ &\times\left(\frac{m_a}{10^{-13}\,{\rm eV}}\right)^2\left(\frac{\rho_{\rm DM}}{0.3\,{\rm GeV/cm^3}}\right).\end{aligned} \tag{10}$$

where ρ_a and $\rho_{\rm DM}$ are the energy densities of axions and dark matter. We defined the effective coupling parameter,

$$\ell_{\rm eff} := \ell f_{\rm DM}^{1/4}, \tag{11}$$

including the fraction of the amount of axions to the total amount of dark matter, $f_{\rm DM} := \rho_a/\rho_{\rm DM}$.

Figure 1 is an example for the signal delay and duration compared with the time to merger for various compact binaries. When the delay is longer than the time to merger, the axion signal is observed after the binary merger ($m_a \gtrsim 10^{-13}\,{\rm eV}$ in Fig. 1).

B. Amplitude enhancement of secondary GWs

We are surrounded by the MW dark matter halo with the size R. Since axions form clouds [32] with the L_c, the MW halo contains many axion patches. The number of patches, N, along the propagation path of a GW is estimated to be

$$N = R/L_c = 2.5\times10^{11}\left(\frac{R}{100\,\mathrm{kpc}}\right)\left(\frac{\Delta v}{10^{-3}}\right)\left(\frac{m_a}{10^{-13}\,\mathrm{eV}}\right) . \quad (12)$$

In the MW halo, GWs from CBC induce the decay of axions into monochromatic GWs at the frequency, $f_{\rm res}$. In other words, the propagating GW is amplified in each axion patch by a factor of $1+\delta_{\rm patch}$ [32], where

$$\delta_{\rm patch} = \frac{1}{2}\left(\frac{\sqrt{\pi G\rho_a}\ell^2 m_a^2}{2}L_{\rm c}\right)^2 \mathrm{sinc}^2\left(2\pi\frac{f-f_{\rm res}}{\Delta f_{\rm res}}\right). \quad (13)$$

The authors of [32] neglect the phase rotation of the GW propagating through each axion patch because it is tiny. In the case, the amplification in each patch is treated coherently and the GW amplitude grows exponentially, giving the amplification factor of $[(1+\delta_{\rm patch})e^{i\theta}]^N \simeq e^{N\delta_{\rm patch}}$ for sufficiently large N and tiny phase shift θ for the secondary GW (see Supplemental material). However, the statement is not true for the entire MW halo. Because the number of patches N is very large and the tiny phase shift θ is accumulated during propagation in the MW halo, the total phase shift finally reaches the limit beyond which the GW is no longer enhanced coherently. Such imperfect amplification has been numerically simulated in the time domain in [39], but for the first time we derive the analytical formula below.

Since a secondary GW is almost monochromatic with the width $\Delta f_{\rm res}$, let us consider the two frequency modes at the edges of the resonance, that is, at $f_{\rm res}+\Delta f_{\rm res}$ and $f_{\rm res}-\Delta f_{\rm res}$. If the phase difference accumulates over π, those modes suppress each other incoherently. Then, the phase shift is accumulated coherently during the period $\Delta t_{\rm coh}$ defined by $2\pi(2\Delta f_{\rm res})\Delta t_{\rm coh}=\pi$, that is, $\Delta t_{\rm coh} = 1/(4\Delta f_{\rm res}) = L_{\rm c}/4$. When propagating in $\Delta t_{\rm coh}$, a secondary GW passes the number of patches $N_{\rm c}$:

$$N_{\rm c} := N\frac{\Delta t_{\rm coh}}{\Delta t_{\rm delay}} , \quad (14)$$

because the delay from one axion patch is $\Delta t_{\rm delay}/N$. If $N_{\rm c} > N$, the enhancement occurs coherently in all patches. However, in the case of $N_{\rm c} < N$, the resonant growth stops after passing $N_{\rm c}$ patches and the total enhancement is given by an incoherent superposition of $N/N_{\rm c}$ enhanced GWs. The total enhancement factor is given by

$$F_{\rm halo} \simeq \begin{cases} e^{N\delta_{\rm patch}} & \text{for } N_{\rm c}\geq N \\ e^{N_{\rm c}\delta_{\rm patch}}\sqrt{\dfrac{N}{N_{\rm c}}} & \text{for } N_{\rm c}<N \end{cases} . \quad (15)$$

with

$$N\delta_{\rm patch} = \frac{\pi^2 G}{4}\frac{R m_a^3\ell^4\rho_a}{\Delta v}\left\langle \mathrm{sinc}^2\left(2\pi\frac{f-f_{\rm res}}{\Delta f_{\rm res}}\right)\right\rangle \quad (16)$$

$$= 9.3\left(\frac{10^{-3}}{\Delta v}\right)\left(\frac{R}{100\,\mathrm{kpc}}\right)\left(\frac{m_a}{10^{-13}\,\mathrm{eV}}\right)^3 \left(\frac{\ell_{\rm eff}}{10^8\,\mathrm{km}}\right)^4\left(\frac{\rho_{\rm DM}}{0.3\,\mathrm{GeV/\,cm^3}}\right) , \quad (17)$$

$$N_{\rm c}\delta_{\rm patch} = \frac{3}{8} . \quad (18)$$

where the sinc factor is averaged for $|f-f_{\rm res}| < \Delta f_{\rm res}$ because GWs are amplified in the narrow range, $\left\langle \mathrm{sinc}^2\left(2\pi\frac{f-f_{\rm res}}{\Delta f_{\rm res}}\right)\right\rangle = 0.24$. The critical case is $N=N_{\rm c}$, that is, from Eqs. (17) and (18), the critical coupling is

$$\ell_c^{\rm eff} = 4.5\times10^7\,\mathrm{km}\left(\frac{\Delta v}{10^{-3}}\right)^{1/4}\left(\frac{100\,\mathrm{kpc}}{R}\right)^{1/4} \left(\frac{10^{-13}\,\mathrm{eV}}{m_a}\right)^{3/4}\left(\frac{0.3\,\mathrm{GeV/\,cm^3}}{\rho_{\rm DM}}\right)^{1/4} . \quad (19)$$

In the left panel of Fig. 2, the coherent ($\theta=0$) and realistic enhancement factors are plotted as a function of $N/N_{\rm c}$ for illustration. It is shown that neglecting the phase shift θ in each axion patch significantly overestimates the enhancement factor for $N > N_{\rm c}$. In the right panel of Fig. 2, the realistic enhancement factor in Eq. (15) is plotted as a function of m_a and $\ell_{\rm eff}$. Even for the realistic case, the enhancement factor can be significantly large for large $N/N_{\rm c}$ (the upper right region).

III. METHOD

In this section, a search method optimized for axion signals is explained. If an axion signal is in data, it should be almost a monochromatic wave at the frequency of $f_{\rm res}$ for a time duration $\Delta t_{\rm duration}$ starting at $\Delta t_{\rm delay} - \tau(f_{\rm res})$ from the coalescence time, where the time to merger is $\tau(f) = (5/256)(\pi f)^{-8/3}\left(G\mathcal{M}/c^3\right)^{-5/3}$ and $\mathcal{M}$ is the chirp mass. For the axion mass range that we search, $1.7\times10^{-13}\,\mathrm{eV} < m_a < 8.5\times10^{-12}\,\mathrm{eV}$, the time to merger is negligible compared with the delay time so that the starting time of the secondary GW is almost at $\Delta t_{\rm delay}$ from the coalescence time. The Fourier amplitude of the secondary signal is given by

$$\left|\tilde{h}_{\rm axion}(f_{\rm res})\right| = [F_{\rm halo}(f_{\rm res})-1]\left|\tilde{h}_{\rm CBC}(f_{\rm res})\right| , \quad (20)$$

where $\tilde{h}_{\rm CBC}(f)$ is the Fourier amplitude of a primary GW signal from a CBC. For $\tilde{h}_{\rm CBC}$ of BBH, we use the IMRPhenomD waveform [40, 41], which is an aligned-spinning inspiral-merger-ringdown waveform, setting the high frequency cutoff to the peak frequency at which the amplitude of the waveform is maximized. While for BNS,

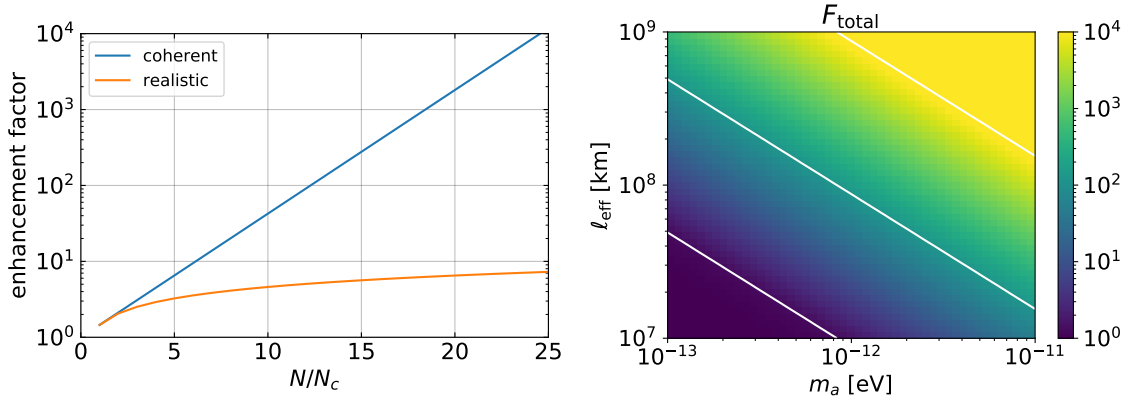


FIG. 2. Left: the coherent ($\theta = 0$) (blue) and realistic (orange) enhancement factors as a function of N/N_c. Right: the realistic enhancement factor as a function of m_a and $\ell_{\rm eff}$. The white diagonal lines from the bottom to the top are the coupling strengths of $N/N_c = 1$ (the critical coupling), 10^4, and 10^8.

the waveform is not accurate enough for high frequencies because of tidal deformation and the high-frequency cut-off is set to the innermost stable circular orbit (ISCO) frequency for a Schwarzchild black hole (BH). When obtaining the CBC amplitude, we need the distance to the GW source and the antenna responses at the time of each event. For conservative constraints, the farthest distance within the 1σ error is used [42]. As discussed in Supplemental material, the difference of the antenna responses hardly affects the results. The events used in this paper are enumerated later, and the data are downloaded from [42]. The other waveform parameters (e.g. the chirp mass, inclination angle, right ascension, declination, and so on) are set to the maximum-likelihood values.

To search the axion signals, we do following steps.

1. Make the $\chi^2_{\rm obs}$ map on the m_a–$\ell_{\rm eff}$ plane from whitened data:
   $\chi^2_{\rm obs} \coloneqq \sum_{I\in{\rm IFO}} \left|\tilde{d}_I(f_{\rm res})\sqrt{\Delta f}/\sqrt{S_{n,I}(f_{\rm res})}\right|^2$,
   where $\tilde{d}_I$ is the Fourier amplitude of the data starting at $\Delta t_{\rm delay}$ from the coalescence time with the chunk size of $\Delta t_{\rm duration}$, $S_{{\rm n},I}(f)$ is the power spectral density (PSD) for I-th detector, and Δf is the width of a frequency bin.
   (a) Take a chunk of whiten data with the duration equal to $\Delta t_{\rm duration}(m_a)$ from $\Delta t_{\rm delay}(m_a, \ell_{\rm eff})$ for a set of the parameters $(m_a, \ell_{\rm eff})$.
   (b) Calculate the $\chi^2_{\rm obs}$ at $f_{\rm res}$.
   (c) Repeat (1a) and (1b) for other $(m_a, \ell_{\rm eff})$.

2. Make a p-value map on the m_a–$\ell_{\rm eff}$ plane from the $\chi^2_{\rm obs}$ map. The p-value to reject the $\ell_{\rm eff}$ is
   $$p(m_a, \ell_{\rm eff}) \coloneqq \int_0^{\chi^2_{\rm obs}} p_\chi\left(x|\overline{\chi^2}\right) {\rm d}x \qquad (21)$$
   where $\overline{\chi^2} \coloneqq \sum_{I\in{\rm IFO}} |\tilde{h}_{\rm axion}(f_{\rm res})\sqrt{\Delta f}/\sqrt{S_{n,I}(f_{\rm res})}|^2$. For example, the p-value is tiny when the expectation value of the non-central χ^2-distribution is much larger than the actually observed one.

3. Search for parameter sets, $(m_a, \ell_{\rm eff})$, for which the p-value is larger than a threshold, that is, judge if there exists the axion signal. We set the threshold to 5×10^{-3} or at 0.5% credible level.

4. Combine the search results from multiple GW events to check consistency among all GW events. Logical OR of non-detection is used to combine the results. That is, if the parameter sets are rejected even by one GW event, they are also rejected in the combined result. Then we derive upper limits on $\ell_{\rm eff}$ for each m_a.

As the constraints are combined for multiple GW events, the constraint on the $\ell_{\rm eff}$ becomes always tighter with more events. However, if the axion signal exists, the true parameter set cannot be rejected even if the number of the combined GW events is large enough.

Since the GW detectors, LIGO and Virgo [48], are sensitive at 20 Hz–1024 Hz, we search the corresponding mass range, $1.7 \times 10^{-13}\,{\rm eV} < m_a < 8.5 \times 10^{-12}\,{\rm eV}$, in this paper. However, the axion signal does not exist beyond the peak frequency because no primary GW exists as in Eq. 20. Thus, for each GW event, we search the axion signal up to the peak frequency. However, since we use the IMRPhenomD waveform up to the ISCO frequency for BNS, the cutoff frequency GW170817 is given by the ISCO frequency.

For this search to constrain the wide parameter range, we need the data that last longer after the amplitude peak of primary GWs and that are available from all detectors (LIGO-Hanford, LIGO-Livingston, and Virgo). We require the length of the data about 5.3×10^4 s for GW170814 [44], GW170817 [45, 46],

TABLE I. Properties of primary GWs analyzed in this paper. The frequency cutoff is set to 1024 Hz for the peak frequency > 1024 Hz.

event name	primary mass $[M_\odot]$	secondary mass $[M_\odot]$	frequency cutoff [Hz]	network SNR of a primary GW	duty cycle of the data used	references
GW170814	31	25	5.9×10^2	16	92%	[43, 44]
GW170817	1.5	1.3	8.0×10^2	33	79%	[43, 45, 46]
GW190728_064510	12	8.1	1.0×10^3	14	61%	[47]
GW200202_154313	10	7.3	1.0×10^3	11	97%	[47]
GW200316_215756	13	7.8	1.0×10^3	10	100%	[47]

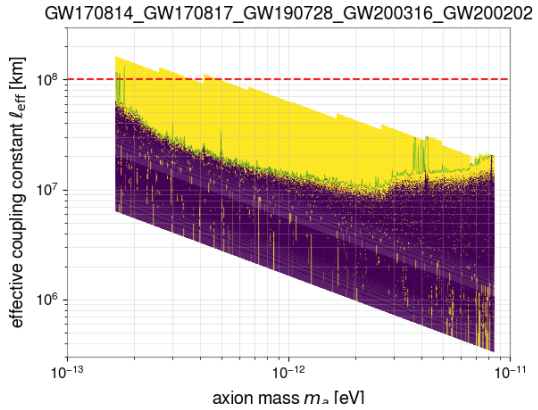


FIG. 3. Constraint on the $\ell_{\rm eff}$ as a function of m_a. The yellow region is rejected at more than 99.5% level, the purple one is not excluded, and the white one is not searched. The green line is an upper limit and the red dashed one is the previous constraint from Gravity Probe B for $f_{\rm DM} = 1$.

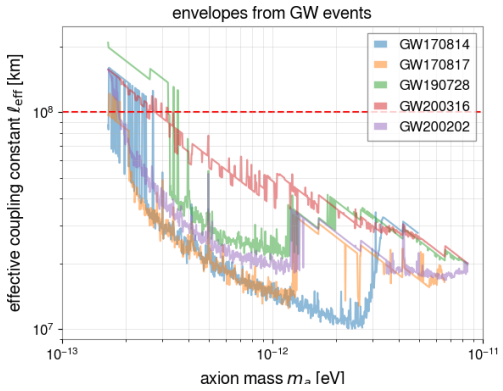


FIG. 4. Minimum values of $\ell_{\rm eff}$ constrained at more than 99.5% level from each GW event in Table I. The red dashed line is the previous constraint from Gravity Probe B for $f_{\rm DM} = 1$.

and GW190728_064510 [43], and about 1.2×10^4 s for GW200202_154313 and GW200316_215756 [47], which are determined from computational time and the less fraction of data lack (see Supplemental material). Furthermore, for the third observing run (O3) events, we require the network signal-to-noise ratio (SNR) higher than 10 and the peak frequency higher than 1024 Hz. The GW events satisfying the conditions are listed in Table I.

IV. RESULTS

Figure 3 shows the search result from the events listed in Table I. The yellow region is excluded at 99.5% credible level, but the purple is not. The white region is not searched. The reason is discussed in the next section. The green line is an upper limit of the constraint, which is the maximum of $\ell_{\rm eff}$ not excluded in the coupling parameter searched. Since there are many points sparsely distributed on the $(m_a, \ell_{\rm eff})$ plane that were not ruled out due to accidental noise fluctuations, we consider the envelope to obtain conservative upper limits on the coupling $\ell_{\rm eff}$ for each m_a. The upper limit has some peaks. Those are caused by detector line noises. The red dashed line is the previous constraint from Gravity Probe B [33]. The constraint is improved by at most one order of magnitude from the Gravity Probe B. The upper shape of the yellow region is like a saw. This is because the search is performed from weaker to stronger couplings until the unsearched $\ell_{\rm eff}$ or $\Delta t_{\rm delay}$ is encountered. For larger $\ell_{\rm eff}$ or longer time delay, the data chunk searched is far from the event time of the primary GW, and the detector data are more likely to be in the non-science mode.

Figure 4 shows the minimum values of $\ell_{\rm eff}$ that were ruled out from each GW event in Table I. In Fig. 4, there are many step-function-like jumps of the lines. This is due to short duration noises. Since $\Delta t_{\rm delay} \propto m_a^2 \ell_{\rm eff}^4$, the search with the mass heavier than that at which the jump exists always encounters the short duration noise and gives almost the same largest $\ell_{\rm eff}$ not excluded. On the other hand, in the search with lighter masses, we can neglect the short duration noise because the contribution is diluted enough due to longer duration of the chunks. Although the highest SNR event is GW170817, the strongest constraint is obtained from GW170814. This is because, even though the SNR is lower, the amplitude of a primary GW is larger for BBH events, producing a larger secondary GW.

V. DISCUSSIONS

The constraints are obtained for the MW dark matter halo parameters, $R = 100\,{\rm kpc}, \Delta v = 10^{-3}$, and $\rho_{\rm DM} =$

$0.3\,\mathrm{GeV/cm^3}$, but these measurement values should have large uncertainties. Nevertheless, the effects on our results are expected to be small, because the dependence of $\ell_{\rm eff}$ on the halo parameters is the power of 1/4 from Eq. (19). Given the uncertainties of $\mathcal{O}(10\%)$ [49] in the MW dark matter halo parameters, they modify $\ell_{\rm eff}$ by the order of $\mathcal{O}(1\%)$. Although we assume that the halo is homogeneous in this paper, we could consider a realistic halo density profile, which is more dense at the center and coarse at the edge [35, 50]. However, it is beyond the scope of this paper.

Our constraint is stronger than that in [32]. Their method is simply to set the condition, $\chi_{\rm obs} > 100$, for detection. The threshold corresponds to $F_{\rm total} \sim 100$ in Fig. 2. Our detection threshold is roughly $F_{\rm total} \sim 5$–50 and much smaller thanks to statistically evaluating the χ^2-value and combining multiple events. Thus the difference of the constraints is from that of the detection criteria.

Also, there is another constraint from the observation of a neutron star with NICER [51]. Although the constraint looks much stronger than ours, it is not obvious for some assumptions in [51] to be satisfied for $\ell \sim 10^8\,\mathrm{km}$. Differences between our and their constraints are discussed in Supplemental material.

Future GW detectors are more sensitive than or have the sensitive frequency bands different from that of the current GW detectors. However, as discussed in Supplemental material, we cannot expect a significant improvement of the constraint on the coupling due to weak dependence on GW amplitude.

VI. CONCLUSIONS

GWs from CBCs are delayed and amplified during the propagation in an axion dark matter halo. In this paper, we have derived a realistic enhancement of the secondary GW amplitude, taking into account the accumulation of a phase delay during propagation and searched such signals with characteristic duration and time delay in the GW observational data. Since we know the signal duration and the time delay of axion signal, we take the data chunk whose length is the same as the duration at the time delay after a binary merger. In the search, we use the data right after the five reported GWs from CBCs. Then, since the signal duration and the time delay depend on the axion mass and the CS coupling, we analyze the data chunk and constraint the coupling by comparing the search result with the expected amplitude of the secondary GW. The constraint on the effective coupling constant $\ell_{\rm eff}$ for axion mass in the range of $[1.65 \times 10^{-13}, 8.47 \times 10^{-12}]$ eV is at most ~ 10 times improved from the previous study, Gravity Probe B [33].

ACKNOWLEDGMENTS

We thank S. Morisaki for fruitful discussions and valuable comments on the draft of the paper. T. T. is supported by JSPS KAKENHI Grant No. 21J12046. A. N. is supported by JSPS KAKENHI Grant Nos. JP19H01894 and JP20H04726 and by Research Grants from Inamori Foundation. The authors are grateful for computational resources provided by the LIGO Laboratory and supported by National Science Foundation Grants PHY-0757058 and PHY-0823459. This material is based upon work supported by NSF's LIGO Laboratory which is a major facility fully funded by the National Science Foundation.

[1] R. D. Peccei and Helen R. Quinn. CP Conservation in the Presence of Pseudoparticles. *Phys. Rev. Lett.*, 38:1440–1443, Jun 1977. 1

[2] C. A. Baker, D. D. Doyle, P. Geltenbort, K. Green, M. G. D. van der Grinten, P. G. Harris, P. Iaydjiev, S. N. Ivanov, D. J. R. May, J. M. Pendlebury, J. D. Richardson, D. Shiers, and K. F. Smith. Improved Experimental Limit on the Electric Dipole Moment of the Neutron. *Phys. Rev. Lett.*, 97:131801, Sep 2006. 1

[3] Asimina Arvanitaki, Savas Dimopoulos, Sergei Dubovsky, Nemanja Kaloper, and John March-Russell. String axiverse. *Phys. Rev. D*, 81:123530, Jun 2010. 1

[4] Igor G. Irastorza and Javier Redondo. New experimental approaches in the search for axion-like particles. *Prog. Part. Nucl. Phys.*, 102:89–159, 2018. 1

[5] Pierre Sikivie. Invisible Axion Search Methods. *Rev. Mod. Phys.*, 93(1):015004, 2021. 1

[6] Jack W. Brockway, Eric D. Carlson, and Georg G. Raffelt. SN 1987A gamma-ray limits on the conversion of pseudoscalars. *Physics Letters B*, 383(4):439–443, 1996. 1

[7] Christopher S. Reynolds, M. C. David Marsh, Helen R. Russell, Andrew C. Fabian, Robyn Smith, Francesco Tombesi, and Sylvain Veilleux. Astrophysical Limits on Very Light Axion-like Particles from Chandra Grating Spectroscopy of NGC 1275. *The Astrophysical Journal*, 890(1):59, feb 2020. 1

[8] John Preskill, Mark B. Wise, and Frank Wilczek. Cosmology of the invisible axion. *Physics Letters B*, 120(1):127–132, 1983. 1

[9] L.F. Abbott and P. Sikivie. A cosmological bound on the invisible axion. *Physics Letters B*, 120(1):133–136, 1983.

[10] Michael Dine and Willy Fischler. The not-so-harmless axion. *Physics Letters B*, 120(1):137–141, 1983.

[11] Zurab Berezhiani and Maxim Yu. Khlopov. Cosmology of spontaneously broken gauge family symmetry with axion solution of strong CP-problem. *Zeitschrift für Physik C Particles and Fields*, 49:73–78, 1991.

[12] Z. G. Berezhiani, A. S. Sakharov, and M. Yu. Khlopov. Primordial background of cosmological axions. *Soviet Journal of Nuclear Physics*, 55(7):1063–1071, July 1992.

[13] A. S. Sakharov, D. D. Sokoloff, and M. Yu. Khlopov. Large-scale modulation of the distribution of coherent oscillations of a primordial axion field in the universe. *Physics of Atomic Nuclei*, 59(6):1005–1010, June 1996.

[14] M.Yu. Khlopov, A.S. Sakharov, and D.D. Sokoloff. The nonlinear modulation of the density distribution in standard axionic CDM and its cosmological impact. *Nuclear Physics B - Proceedings Supplements*, 72:105–109, 1999. Proceedings of the 5th IFT Workshop on Axions.

[15] A.S. Sakharov and M.Yu. Khlopov. The nonhomogeneity problem for the primordial axion field. *Physics of Atomic Nuclei*, 57:485–487, 1994.

[16] Fabio Moretti, Flavio Bombacigno, and Giovanni Montani. Gravitational Landau damping for massive scalar modes. *The European Physical Journal C*, 80(12), dec 2020. 1

[17] Francesca Chadha-Day, John Ellis, and David J. E. Marsh. Axion dark matter: What is it and why now? *Sci. Adv.*, 8(8):abj3618, 2022. 1

[18] Luca Di Luzio, Maurizio Giannotti, Enrico Nardi, and Luca Visinelli. The landscape of QCD axion models. *Phys. Rept.*, 870:1–117, 2020.

[19] Giorgio Galanti and Marco Roncadelli. Axion-like Particles Implications for High-Energy Astrophysics. *Universe*, 8(5):253, 2022. 1

[20] Stephon Alexander and Nicolás Yunes. Chern–Simons modified general relativity. *Physics Reports*, 480(1-2):1–55, aug 2009. 1

[21] Renée Hložek, David J E Marsh, and Daniel Grin. Using the full power of the cosmic microwave background to probe axion dark matter. *Monthly Notices of the Royal Astronomical Society*, 476(3):3063–3085, 02 2018. 1

[22] David J. E. Marsh and Pedro G. Ferreira. Ultralight scalar fields and the growth of structure in the Universe. *Phys. Rev. D*, 82:103528, Nov 2010.

[23] Andrei Khmelnitsky and Valery Rubakov. Pulsar timing signal from ultralight scalar dark matter. 2014(02):019–019, feb 2014.

[24] N. K. Porayko and K. A. Postnov. Constraints on ultralight scalar dark matter from pulsar timing. *Phys. Rev. D*, 90:062008, Sep 2014.

[25] Arata Aoki and Jiro Soda. Pulsar timing signal from ultralight axion in $f(R)$ theory. *Phys. Rev. D*, 93:083503, Apr 2016.

[26] Arata Aoki and Jiro Soda. Detecting ultralight axion dark matter wind with laser interferometers. *International Journal of Modern Physics D*, 26(07):1750063, Dec 2016.

[27] Arata Aoki and Jiro Soda. Nonlinear resonant oscillation of gravitational potential induced by ultralight axion in $f(R)$ gravity. *Phys. Rev. D*, 96:023534, Jul 2017.

[28] Diego Blas, Diana López Nacir, and Sergey Sibiryakov. Ultralight Dark Matter Resonates with Binary Pulsars. *Phys. Rev. Lett.*, 118:261102, Jun 2017.

[29] Asimina Arvanitaki and Sergei Dubovsky. Exploring the string axiverse with precision black hole physics. *Phys. Rev. D*, 83:044026, Feb 2011.

[30] Hirotaka Yoshino and Hideo Kodama. The bosenova and axiverse. 32(21):214001, oct 2015.

[31] C. Abel, N. J. Ayres, et al. Search for Axionlike Dark Matter through Nuclear Spin Precession in Electric and Magnetic Fields. *Phys. Rev. X*, 7:041034, Nov 2017.

[32] Sunghoon Jung, TaeHun Kim, Jiro Soda, and Yuko Urakawa. Constraining the gravitational coupling of axion dark matter at LIGO. *Phys. Rev. D*, 102:055013, Sep 2020. 1, 2, 3, 6

[33] Yacine Ali-Haimoud and Yanbei Chen. Slowly-rotating stars and black holes in dynamical Chern-Simons gravity. *Phys. Rev. D*, 84:124033, 2011. 1, 5, 6

[34] Daiske Yoshida and Jiro Soda. Exploring the string axiverse and parity violation in gravity with gravitational waves. *International Journal of Modern Physics D*, 27(09):1850096, Jul 2018. 1

[35] Gaetano Lambiase, Leonardo Mastrototaro, and Luca Visinelli. Chern-simons axion gravity and neutrino oscillations. 2022. 1, 6

[36] Benjamin V Church, Philip Mocz, and Jeremiah P Ostriker. Heating of Milky Way disc stars by dark matter fluctuations in cold dark matter and fuzzy dark matter paradigms. *Monthly Notices of the Royal Astronomical Society*, 485(2):2861–2876, 02 2019. 2

[37] J Aasi, B P Abbott, R Abbott, T Abbott, M R Abernathy, K Ackley, C Adams, T Adams, P Addesso, et al. Advanced LIGO. *Classical and Quantum Gravity*, 32(7):074001, Mar 2015. 2

[38] Gregory M Harry. Advanced LIGO: the next generation of gravitational wave detectors. *Classical and Quantum Gravity*, 27(8):084006, apr 2010. 2

[39] Tomohiro Fujita, Ippei Obata, Takahiro Tanaka, and Kei Yamada. Resonant gravitational waves in dynamical Chern–Simons–axion gravity. *Classical and Quantum Gravity*, 38(4):045010, dec 2020. 3

[40] Sascha Husa, Sebastian Khan, Mark Hannam, Michael Pürrer, Frank Ohme, Xisco Jiménez Forteza, and Alejandro Bohé. Frequency-domain gravitational waves from nonprecessing black-hole binaries. I. New numerical waveforms and anatomy of the signal. *Phys. Rev. D*, 93:044006, Feb 2016. 3

[41] Sebastian Khan, Sascha Husa, Mark Hannam, Frank Ohme, Michael Pürrer, Xisco Jiménez Forteza, and Alejandro Bohé. Frequency-domain gravitational waves from nonprecessing black-hole binaries. II. A phenomenological model for the advanced detector era. *Phys. Rev. D*, 93:044007, Feb 2016. 3

[42] Gravitational Wave Open Science Center. `https://www.gw-openscience.org`. 4

[43] R. Abbott, T. D. Abbott, et al. GWTC-2: Compact Binary Coalescences Observed by LIGO and Virgo during the First Half of the Third Observing Run. *Phys. Rev. X*, 11:021053, Jun 2021. 5

[44] B. P. Abbott, R. Abbott, T. D. Abbott, F. Acernese, K. Ackley, C. Adams, T. Adams, P. Addesso, R. X. Adhikari, V. B. Adya, et al. GW170814: A Three-Detector Observation of Gravitational Waves from a Binary Black Hole Coalescence. *Physical Review Letters*, 119(14), Oct 2017. 4, 5

[45] B. P. Abbott, R. Abbott, T. D. Abbott, F. Acernese, K. Ackley, C. Adams, T. Adams, P. Addesso, R. X. Adhikari, V. B. Adya, et al. GW170817: Observation of Gravitational Waves from a Binary Neutron Star Inspiral. *Physical Review Letters*, 119(16), Oct 2017. 4, 5

[46] B. P. Abbott et al. Multi-messenger Observations of a Binary Neutron Star Merger. *Astrophys. J.*, 848(2):L12, 2017. 4, 5

[47] R. Abbott et al. GWTC-3: Compact Binary Coalescences Observed by LIGO and Virgo During the Second Part of the Third Observing Run. 11 2021. 5

[48] F Acernese, M Agathos, K Agatsuma, D Aisa, N Allemandou, A Allocca, J Amarni, P Astone, G Balestri, G Ballardin, et al. Advanced Virgo: a second-generation interferometric gravitational wave detector. *Classical and Quantum Gravity*, 32(2):024001, Dec 2015. 4

[49] Elisa G. M. Ferreira. Ultra-light dark matter. *The Astronomy and Astrophysics Review*, 29(1), sep 2021. 6

[50] Julio F. Navarro, Carlos S. Frenk, and Simon D. M. White. The Structure of Cold Dark Matter Halos. *The Astrophysical Journal*, 462:563, may 1996. 6

[51] Hector O. Silva, A. Miguel Holgado, Alejandro Cárdenas-Avendaño, and Nicolás Yunes. Astrophysical and Theoretical Physics Implications from Multimessenger Neutron Star Observations. *Phys. Rev. Lett.*, 126:181101, May 2021. 6

[52] Nicolás Yunes, Dimitrios Psaltis, Feryal Özel, and Abraham Loeb. Constraining parity violation in gravity with measurements of neutron-star moments of inertia. *Phys. Rev. D*, 81:064020, Mar 2010.

[53] Semih Tuna, Kıvanç İ. Ünlütürk, and Fethi M. Ramazanoğlu. Constraining scalar-tensor theories using neutron star mass and radius measurements, 2022.

[54] M Punturo et al. The Einstein Telescope: a third-generation gravitational wave observatory. *Classical and Quantum Gravity*, 27(19):194002, sep 2010.

[55] Michele Maggiore, Chris Van Den Broeck, Nicola Bartolo, Enis Belgacem, Daniele Bertacca, Marie Anne Bizouard, Marica Branchesi, Sebastien Clesse, Stefano Foffa, Juan García-Bellido, et al. Science case for the Einstein telescope. *Journal of Cosmology and Astroparticle Physics*, 2020(03):050–050, Mar 2020.

[56] B P Abbott et al. Exploring the sensitivity of next generation gravitational wave detectors. *Classical and Quantum Gravity*, 34(4):044001, jan 2017.

[57] Sheila Dwyer, Daniel Sigg, Stefan W. Ballmer, Lisa Barsotti, Nergis Mavalvala, and Matthew Evans. Gravitational wave detector with cosmological reach. *Phys. Rev. D*, 91:082001, Apr 2015.

[58] Stanislav Babak, Martin Hewitson, and Antoine Petiteau. LISA Sensitivity and SNR Calculations, 2021.

[59] Seiji Kawamura, Takashi Nakamura, et al. The Japanese space gravitational wave antenna—DECIGO. *Classical and Quantum Gravity*, 23(8):S125–S131, mar 2006.

[60] Seiji Kawamura, Masaki Ando, et al. The Japanese space gravitational wave antenna: DECIGO. *Classical and Quantum Gravity*, 28(9):094011, apr 2011.

[61] G. Hobbs, A. Archibald, Z. Arzoumanian, et al. The International Pulsar Timing Array project: using pulsars as a gravitational wave detector. *Classical and Quantum Gravity*, 27(8):084013, April 2010.